JOURNAL OF OPTOELECTRONICS AND ADVANCED MATERIALS, Vol. 11, No. 9, September 2009, p. 1157 - 1162

The thermal spike model of polyimide erosion by low energy ion bombardment♣

ILARIA DI SARCINA, SALVATORE SCAGLIONE*
ENEA, Advanced Physics Technology And New Materials Department,Optical Coatings Grou,CR Casaccia, Via Anguillarese 301,00123 Rome, Italy

Low energy ions are used for different applications such as ion beam assistance, surface modification of materials, ground simulation of space, etc. In this paper, polyimide (Dupont Kapton™) sheets were bombarded by an ion beam produced by an End-Hall ion source. The erosion rate, measured at the masking part of the Kapton target, was measured with varying source parameters. Two set of samples were bombarded with argon and oxygen ions. The erosion mechanism was explained by assuming that a low energy ion comes to rest a few monolayers from the Kapton surface. Most of the ion energy is released as phonons and a thermal spike is generated. According to the physics of the SRIM (Stopping Range of Ions in Matter) code, a thermal spike model was developed and compared with the experimental results. Quite good agreement between the calculated and measured erosion rates was found.

(Received November 5, 2008; accepted December 15, 2008)

Keywords: Low energy ion beam assistance, Thermal spike, Kapton erosion, Atomic oxygen

1. Introduction

Ion bombardment is a widely used technique to modify the material characteristics, to attain technological improvement:

a) ion beam assistance of a growing film, to vary the optical and mechanical properties [1,2,3];

b) ground simulation of surface damage to components undergoing the Low Earth Orbit Space environment [4,5,6];

c) improvement of the substrate adhesion of metallic and dielectric layers [7,8,9].

A knowledge of the parameters influencing the material property changes, under ion bombardment, is useful in simulating the physical mechanisms which govern the ion and matter interaction. The ion mass and energy plays a crucial role in the variation of the surface properties of the bombarded material [10]. In recent years, the use of the low energy ions, from a few eV to a hundred eV, has increased, in order to minimize the damage during the ion treatment process [11,12] . The ions implanted at low energy experience few collisions, and material modification happens even if the ions recoil energy is comparable to the displacement energy E_d (i.e. the energy value necessary to remove an atom from its equilibrium position).

Molecular Dynamics simulations by I. Santos et al. [13], demonstrate that the energy transfers below E_d can produce significant amounts of damage.

The SRIM (Stopping Range of Ions in Matter) code developed by Ziegler, et al. [14] is a group of programs which calculate the stopping and the range of ions in matter (energy range 10 eV – 2 GeV/amu). In the SRIM code, the ions transfer their energy through collisions with atoms and electrons. When the ion energy is equal to or lower than the displacement energy, the ion comes to rest and most of its energy is released as phonons. In the framework of the SRIM assumptions, a thermal spike can be generated in the region around the place where the phonons are released, and the relative position of the atoms within this region can be rearranged [15].

Kapton (polyimide) is very often used in space applications, for its thermal and electrical properties. It is also one of the main materials used in space exposure and ground simulation research. It can be severely eroded by atomic oxygen in LEO orbits [16]. In this work, the erosion phenomenon of a polyimide surface bombarded by argon or oxygen low energy ions is simulated. The model of erosion is based on the physics of the SRIM code, combined with the thermal spike model described in [15]. The results of the simulation are compared with the experimental ones.

♣ Paper presented at the International School on Condensed Matter Physics, Varna, Bulgaria, September 2008

2. SRIM simulations

The SRIM code follows a large number of individual ion histories in an amorphous target. Depending on the status of the target, because SRIM treats in different ways solid or gaseous materials, a correction factor takes into account the bonding change and the target band gap. The scattering process between the ions and the target atoms, and the slowing down of the ions within the matter is simulated by a Monte-Carlo method. The equation of the interaction potential contains a screening function, that for SRIM code is called a "universal" screening function [17,18].

An ion colliding with various atoms in the polyimide target generates a collision cascade (recoils). During this, the ions and the recoils transfer their energy to the lattice, and after several collisions their energies become lower than the displacement energy of the target atoms. Vacancy production, replacement collisions and interstitial atoms are calculated by SRIM, as well as the portion of the energy transferred to the target atoms as phonons and by the ion-atom and atom-atom collisions (recoils).

SRIM simulation of argon ions colliding with atoms of polyimide predicts the behaviour in fig. 1. For ion energies ranging from few eV to 150 eV, most of the ion energy is released to the lattice as phonons.

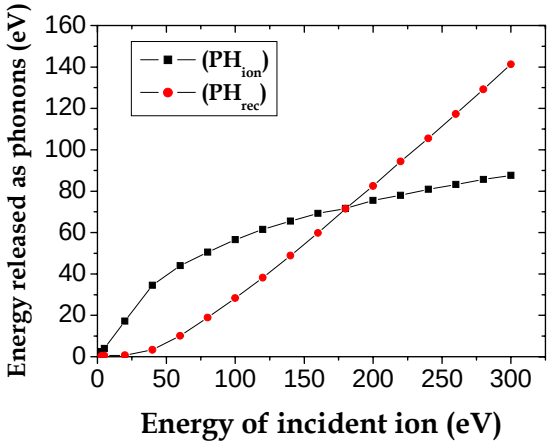

Fig. 1. Ion and recoil energy released as phonons versus the energy of the incident ion.

The energy of ions (ph_{ion}) and recoils (ph_{rec}) released as phonons is transferred to the lattice near the surface. Phonons produced by recoils are released at a depth greater than that for phonons released by the ions. At a low energy of the incident ions, most phonons are produced by the ion itself, near the target surface.

The behaviour of the normalized ion energy PH_{ion} (Eq. 1) transferred as phonons with the ion penetration depth d ; is shown in fig. 2 for different values of the energy of the incident ions.

$$PH_{ion}(d) = \frac{ph_{ion}(d)}{ph_{ion}(d) + ph_{recoil}(d)} \tag{1}$$

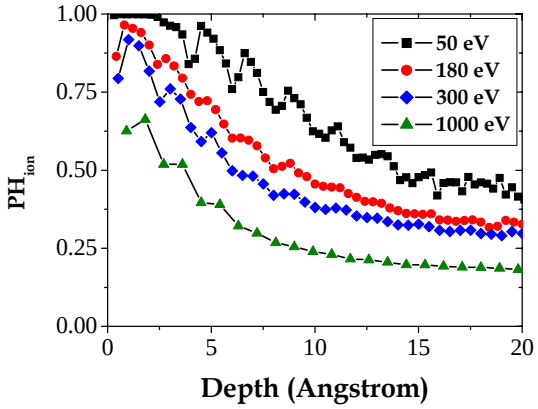

Fig. 2. Normalized ion energy $PH_{ion}(d)$ released to the polyimide lattice as phonons, as a function of the depth.

3. Spherical thermal spike

Depending on the thermal properties of the target, the portion of the ion energy transferred by phonons can generate a thermal spike, high enough to induce a permanent rearrangement of the atoms. The collision process described by SRIM suggests that a spherical symmetry of the temperature spike can be considered. The temperature $T(r,t)$ at a distance r from the centre of the sphere at the time t is [15]:

$$T(r,t) = \frac{E_{ph}(E_{ion})}{8 \cdot \pi^{\frac{3}{2}} \cdot cd} \cdot \frac{1}{(Dt)^{\frac{3}{2}}} \cdot e^{\frac{-r^2}{4 \cdot Dt}} \tag{2}$$

where c and d are the specific heat and the density of polyimide (Kapton) respectively, D is the thermal diffusion coefficient and $E_{ph}(E_{ion})$ is the ion energy transferred as phonons, that depends on the incident ion energy.

A critical spike volume can be defined as the volume in which the atoms posses a high probability of being involved in a rearrangement process. In this volume, the temperature is higher than a critical value T_c. Rearranging Eq. (2), an expression for the critical radius r_c at time t and energy $E_{ph}(E_{ion})$ can be obtained:

$$r_C(t, E_{ion}) = 2 \cdot \left(-\ln\left(4.5 \cdot 10^{-8} \cdot \pi^{\frac{3}{2}} \cdot T_c \, cd \cdot t \, \frac{(D \cdot t)^{\frac{1}{2}}}{E_{ph}(E_{ion})} \right) \cdot D\, t \right)^{\frac{1}{2}} \tag{3}$$

Fig 3 shows curves for three different values of the incident ion energy, calculated by Eq. (3).

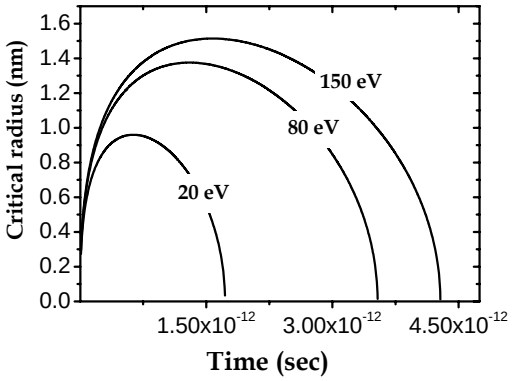

Fig. 3. Critical radius vs. time for three different values of the incident ion energy.

The time t_{max} can be obtained from Eq. (3), with the derivative $\partial r_C/\partial t = 0$.

$$t_{\max}(E_{ion}) = \frac{2.7\cdot 10^4}{\pi\cdot T_C\cdot cd}\cdot\frac{\left(E_{ph}\left(E_{ion}\right)^2\cdot T_C\cdot cd\right)^{\frac{1}{3}}}{D} \qquad (4)$$

Combining Eqs. (4) and (3), the behaviour of the critical radius with the incident ion energy can be described by (see Fig. 4):

$$r_{\max}(E_{ion}) = 2\cdot\left(-\ln\left(A\cdot\pi^{\frac{3}{2}}\cdot T_C\, cd\cdot t_{\max}(E_{ion})\cdot\frac{\left(D\cdot t_{\max}(E_{ion})\right)^{\frac{1}{2}}}{E_{ph}(E_{ion})}\right)\cdot D t_{\max}(E_{ion})\right)^{\frac{1}{2}} \qquad (5)$$

where A is a numerical constant ($4.5\cdot 10^{-8}$).

Fig. 4 shows the behaviour of the critical radius with the energy of the incident Ar ions. A critical sphere where the material damage should be permanent can be calculated by Eq. 5.

In the framework of the spherical thermal spike, it can be supposed that the atoms inside the critical sphere and near the surface can leave the target.

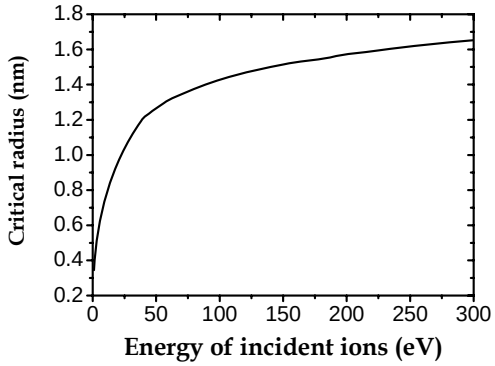

Fig. 4. Critical radius vs. the energy of the incident Ar ions.

Material erosion takes place if the distance between the surface and centre of the critical sphere is equal to or lower than the critical radius. Fig. 5 shows the number of atoms inside the critical sphere when an Ar ion hits the polyimide surface at an energy E_{Ar}. The curves represent the contributions of the ion and recoil energies released as phonons. For energies lower than 70 eV, the erosion is due to the ions. At higher values of the ion energy, the contribution of the recoils increases, and becomes dominant for energies higher than 150 eV.

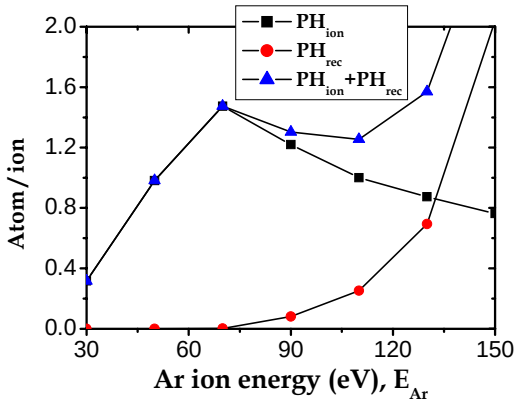

Fig. 5. Number of atoms per incident ion leaving the surface of the polyimide for different Ar ion energies.

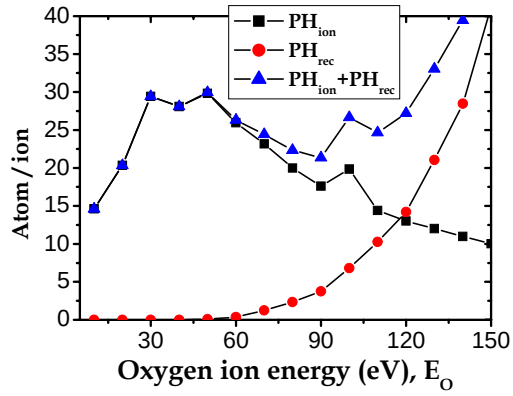

Fig. 6. Number of atoms per incident ion leaving the surface of the polyimide for different oxygen ion energies.

The same simulation was performed using oxygen instead of argon, and the results are shown in Fig. 6. The behaviour of the contribution of ions and recoils with respect to the energy is quite similar to that in Fig. 5. In contrast, the numbers of atoms leaving the surface per incident ion are greater than those simulated with Ar ions. It can be expected that, under similar bombarding conditions, the Kapton material loses more mass when bombarded by oxygen than when bombarded by argon.

4. Experimental

In general, two different classes of ion source are used to produce ion beams: a gridded ion source (Kaufman type) and an End-Hall ion source (gridless type). The main characteristic of the first one is the capability to control the beam energy and dose. In addition, the energy dispersion is very low [19]. The typical energy range of gridded ion sources is between 300 eV and 2 KeV [20]. The ion beam produced by a gridless ion source suffers from a wide energy dispersion with a mean energy ranging from few tenths of eV to a few hundreds of eV [21,22].

For their reliability and low cost, gridless ion sources are ideal candidates for industrial applications where a low ion beam energy and high ion dose are necessary.

Polyimide sheets (Dupont Kapton^{TM}) were bombarded by an ion beam produced by an End-Hall ion source (Advanced Energy, model MARK I). The process chamber was evacuated to a pressure of $2 \cdot 10^{-5}$ Pa, by a cryogenic pump. The bombarding ions were pure oxygen and pure argon. During the erosion process, the working pressure in the chamber was $4 \cdot 10^{-3}$ Pa.

The ions of the beam produced by a gridless ion source have a significant energy spread [16] that depends on the anode voltage and cathode current, V_{anode} and I_{cath}, respectively. Fig. 7 shows the behaviour of the argon ion beam current density obtained by varying the retarding potential of the Faraday cup for $I_{cath}=0.2$ A.

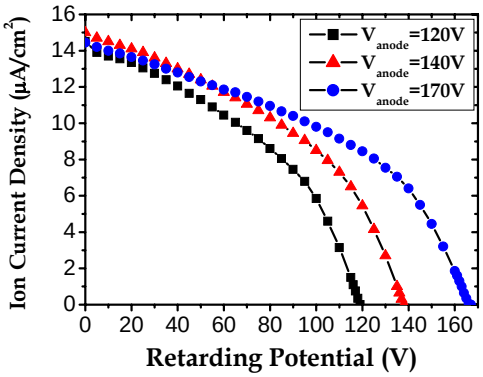

Fig. 7. Density of the Ar ion beam current vs. the retarding potential for three different values of V_{cath}, and $I_{cath}=0.2$ A.

For a singly charged ion, the retarding potential in volts can be translated into ion kinetic energy (in eV) [23]. In the case of oxygen ions, the molecules can break down during the ionization process in the plasma chamber of the ion source. As a consequence, the ion beam can be considered as a mixture of O_2^+ and O^+. In the literature, a value of 0.2 is assigned as the ratio O^+/O_2^+ [4].

For kinetic energies higher than the fragmentation energy (E_f = 18.69 eV) [24] the O_2^+ ions can break during the collision with the atoms of the target surface. As a consequence, the number of the oxygen ions n_{ion} is calculated by the relation $n_{ion}=2 \cdot J \cdot e$ where J is the ion current density and e is the electron charge. The factor of two takes into account the breaking of the molecules of oxygen. The two oxygen atoms resulting from the molecule fragmentation are each considered to have half the energy of the molecule energy.

The energy distribution of the ions was calculated with the derivative dn_{ion}/dE_{ion}. Fig. 8 shows the number of ions/eV at different energies.

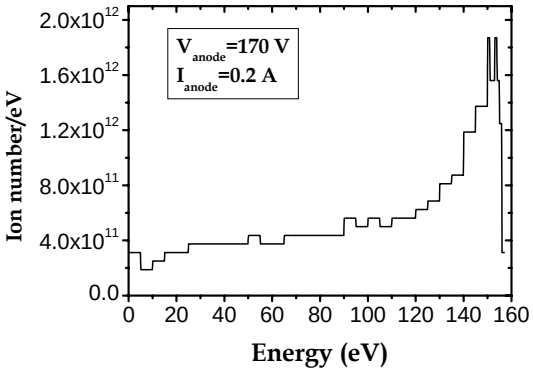

Fig. 8. Dispersion in energy (number of Ar ions per eV) vs. the energy calculated by the derivative of one of the experimental measurements of the ion current density shown in Fig.7.

5. Results and discussion

In order to measure the erosion depth, the samples were partially masked during the bombardment, by a vacuum adhesive tape. Fig. 9 shows a Scanning Electron Microscopy (SEM) picture of a representative Kapton sample.

The step was measured by a surface profilometer (model P8, Tencor Instruments). Fig. 10 shows the step measurement of the sample in Fig. 9.

The properties of the polyimide material are reported in Table 1 [25].

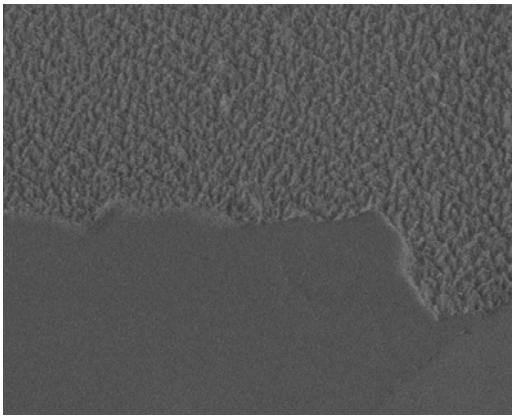

Fig. 9. SEM picture of a Kapton sample. The smooth region (below) is the part of the masked sample after the tape was removed.

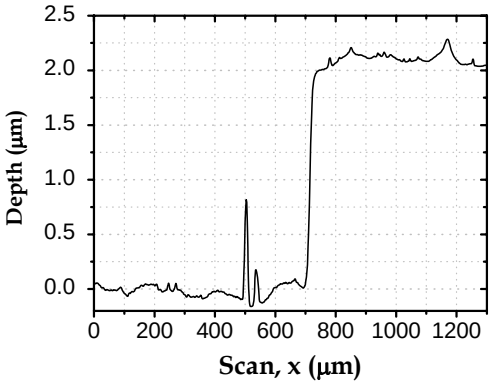

Fig. 10. Profile of the Kapton surface around the masked region.

Table 1. Physical and thermal properties of the polyimide material.

Thermal conductivity C	0.37	$\frac{w}{m \cdot K}$
Specific heat c	1.09×10^{3}	$\frac{J}{Kg \cdot K}$
Mass density d	1.4	$\frac{gr}{cm^3}$
Atomic density ρ	8.7×10^{22}	$\frac{at}{cm^3}$
Thermal diffusion coefficient $D = \frac{C}{c \cdot d}$	2.425×10^{-7}	$\frac{m^2}{\text{sec}}$

6. Erosion rate

The erosion rate for Ar ions was calculated by the equation:

$$r_{Ar} = \int n_{F.C}^{Ar}(E) \cdot n_K(E) \cdot dE \quad \left(\frac{nm}{\text{sec}}\right) \tag{6}$$

where $n_{F.C}^{Ar}(E)$ is the number of argon ions measured by the Faraday Cup, shown in Fig. 8, and $n_K(E)$ is the number of Kapton atoms per incident ion leaving the surface (Fig . 5).

The same procedure can be adopted for oxygen ions:

$$r_{O^+} = 0.2 \cdot \int n_{F.C}^{O_2}(E) \cdot n_K(E) \cdot dE \tag{a}$$

$$r_{O_2^+} = 0.8 \cdot \int 2 \cdot n_{F.C}^{O_2}(E/2) \cdot n_K(E/2) \cdot dE \tag{b}$$

$$r_{oxy} = r_{O^+} + r_{O_2^+} \quad \left(\frac{nm}{\text{sec}}\right) \tag{7}$$

The numerical factors of 0.2 in Eq. (7a) and 2 in Eq. (7b) take into account respectively the percentages of the oxygen molecules which fragment in the plasma ion source, and the ion oxygen molecules breaking when hitting the Kapton atoms with energies higher than E_f.

In Table 2, the experimental and calculated erosion rates (respectively Eqs. (6) and (7)) are compared, for samples bombarded by Ar and oxygen ions.

Table 2. Comparison between the calculated and experimental rates of erosion of a Kapton sheet bombarded by argon and oxygen ions.

V_{anode} (V)	$I_{cathode}$ (A)	r_{calc} (nm/s)	$r_{exp.}$ (nm/s)
170	(Ar^+) 0.20	0.017	0.020
170	(Ar^+) 0.30	0.021	0.022
170	(Ar^+) 0.30	0.016	0.019
140	(O^+/O_2^+) 0.14	0.115	0.077
140	(O^+/O_2^+) 0.20	0.156	0.140
170	(O^+/O_2^+) 0.20	0.148	0.169

Taking into account the poor knowledge of the thermal properties at a nanometre level, the agreement between the calculated and measured erosion rates seems quite good.

7. Conclusions

The SRIM code is a useful instrument for simulating the penetration of ions into matter. For ion energies ranging from a few eV to several hundreds of eV, most of the energy of the ions and of recoils is released as phonons. In the sites where the ions and recoils become at rest (residual energy lower than the atom displacement energy), a thermal spike can occur, causing atomic rearrangement. In this framework, one can define a critical sphere where the rearrangements take place. If this sphere is very close to the surface, the atoms can leave the surface itself.

In this paper, Kapton sheets (polyimide) were bombarded with argon and oxygen ions. The erosion process was simulated by combining the SRIM output data (depth distribution of the energy released as phonons by ions and recoils) with the spherical thermal spike equations.

The calculated and measured erosion rates of the Kapton sheet were compared and, as shown in Table 2, the results were in good agreement.

References

[1] S. Scaglione, D. Flori, L. Caneve, G. Emiliani, J. Vac. Sci. Technol. **A 9(3)**, 1197 (1991).
[2] G. Reisse, S. Weissmantel, B. Keiper, B. Steiger, H.

Johansen, T. Martini, R. Scholz, Applied Surface Science **86**, 107 (1995).
[3] J. Toudert, D. Babonneau, S. Camelio, T. Girardeau, F. Yubero, J. P. Espinòs, R. Gonzalez-Elipe, J. Phys. **D40**, 4614 (2007).
[4] Xiao-Hu Zhao, Zhi-Gang Shen, Yu-Shan Xing, Ahu-Lin Ma, J. Phys. **D34**, 2308 (2001).
[5] E. Grossman, I. Gouzman, Nucl. Instr. and Meth. in Phys. Res. **B208**, 48 (2003).
[6] L. Zhang, T.Yasui, H. Tahara, T. Yoshikawa, J. Appl. Phys. **86**, 779 (1999).
[7] P. Bertrand, P. Lambert, Y. Travaly, Nucl. Instr. and Methods in Phys Res. **B 131**, 71 (1997).
[8] Sung C. Park, Seong S. Yoon, J. D. Nam, Thin Solid Films, **516**, 3028 (2008).
[9] H. G. Jang, K. H. Kim, S. Han, W. K. Choi, H. J. Jung, S. K. Koh, J. Vac. Sci. Technol. **A 15**, 2234 (1997).
[10] O. Auciello, R. Kelly, Ion Bombardment Modification of Surfaces, Elsevier, New York (1984).
[11] Ari Ide-Ektessabi, Nobuto Yasui, Daisuke Okuyama, Review Sci. Instr. **73(2)**, 873 (2002).
[12] Wai-Lun Chan, K. Zhao, N. Vo, Y. Ashkenazy, D. G. Cahill, R. S. Averback, Phys. Rev. B **77**, 205405 (2008).
[13] I. Santos, L.A. Marques, L. Pelaz, Phys. Rew. **B 74**, 174115 (2006).
[14] J. F. Ziegler, SRIM.com, Annapolis, MD, 21037 USA, and J.P.Biersack, Hahn-Meitner Inst. 1 Berlin 39, Germany, program version SRIM-2003.26.
[15] F. Seitz, J. S. Koehler, Solid State Phys. **2**, 305 (1956).
[16] Ph. R. Young, S. S. Wayne, Polymers for Advanced Technologies **9**, 1998, 20-33.
[17] P. Mazzoldi, G. W. Arnold, Ion Beam Modification of Insulators, Elsevier, Amsterdam, 1987.
[18] J. F. Ziegler, J. P. Biersack, M. D. Ziegler, SRIM, The Stopping and Range of Ions in Matter, SRIM co., Chester, Maryland (2008).
[19] A. Anders, Surf and Coat. Technol. **200**, 1893 (2005).
[20] H. R. Kaufman, J. J. Cuomo, J. M. E. Harper, J. Vac. Sci. Technol. **21**, 725 (1982).
[21] D. Tang, L. Wang, S. Pu, C. Cheng, P. K. Chu, Nucl. Instr. Meth. Phys. Res. **257**, 796 (2007).
[22] H. R. Kaufman, R. S. Robinson, Operation of Broad-Beam Sources, Commonwealth Scientific Corporation, Alexandria, Virginia (1987).
[23] H.R. Kaufman, R.S.Robinson, R.I.Seddon, J. Vac. Sci. Technol. A 5 (4), 2081 (1987).
[24] A. N. Zavilopulo, F. F. Chipev, O. B. Shpenik, Technical Physics **50**, 402 (2005).
[25] Datasheet from Dupont web page, http://www2.dupont.com/Kapton/en_US/assets/downloads/pdf/summaryofprop.pdf.

*Corresponding author: salvatore.scaglione@casaccia.enea.it